ATLAS NOTE

ATL-PHYS-PUB-2015-034

10th August 2015

Forward Jet Vertex Tagging: A new technique for the identification and rejection of forward pileup jets

The ATLAS Collaboration[1]

Abstract

The suppression of pileup forward jets is crucial for a variety of physics analyses at the LHC, ranging from VBF Higgs production to SUSY searches. A novel forward pileup tagging technique that exploits the correlation between central and forward jets originating from pileup interactions is presented. Tracking and vertex information in the central η region is used to indirectly tag and reject forward pileup jets that are back-to-back to central pileup jets. The pileup suppression power observed in PYTHIA8 simulated events increases with jet p_{T} and ranges between a 30% and 60% pileup jet removal for 90% jet selection efficiency for jets between 20 and 50 GeV.

[1] The full author list can be found at:
https://atlas.web.cern.ch/Atlas/PUBNOTES/ATL-PHYS-PUB-2014-007/authorlist.pdf

1 Introduction

At the Large Hadron Collider (LHC) the collisions of proton (p) bunches result not only in hard-scatter pp interactions, but also in additional collisions, usually consisting of soft QCD processes. Such additional low transverse momentum pp collisions are referred to as *pileup* interactions. Pileup interactions can be *in-time* or *out-of-time*. In-time pileup arises from additional pp interactions in the same bunch-crossing as the hard-scatter interaction; out-of-time pileup refers to energy deposits in the ATLAS calorimeter [1] from previous and following bunch-crossings with respect to the triggered event. For this note, in-time and out-of-time pileup will be referred collectively as pileup.

The additional transverse energy from pileup interactions is typically subtracted on event-by-event basis from the hard-scatter interaction of interest. Local fluctuations in the pileup activity, however, may result in spurious pileup jets. In Ref. [2] it was shown that pileup jets can be effectively removed using track and vertex information with the jet-vertex-tagger (JVT) technique. A limitation of the JVT discriminant is that it can only be used for jets within the coverage of the inner detector, $|\eta| < 2.5$. However in ATLAS jets are reconstructed over the whole calorimeter coverage, $|\eta| < 4.9$. The suppression of pileup jets in the *forward* region $2.4 < |\eta| < 4.9$ is crucial to enhance the sensitivity of key analyses within the ATLAS physics program, such as single top quark measurements and measurements of Higgs boson production in the Vector Boson Fusion mode.

In this note a technique to identify and reject pileup jets with $|\eta| > 2.4$ is presented. The method exploits the topological correlation between jet pairs produced in pileup interactions. The method is studies using Pythia8 simulation for pileup events. The note is organized as follows. Section 2 briefly describes the ATLAS detector, the object reconstruction and selection. A new method of classifying pileup jets is described in Section 3, while the *forward* JVT technique for suppressing forward pileup jets is presented in Section 4. The performance of the technique is compared in $Z(\rightarrow \mu\mu)$+jets events as well as in $t\bar{t}$ events in Section 5. Finally, the conclusions are discussed in Section 6.

2 Object definition and event selection

2.1 The ATLAS detector

The ATLAS detector is a general purpose particle detector covering almost 4π in solid angle and consisting of an inner tracking detector (ID), a calorimeter, and a muon spectrometer. The details of the detector are given in Ref. [1]. The ID consists of silicon pixel and strip (SCT) tracking detectors covering the pseudorapidity[2] range of $|\eta| < 2.5$ and a straw-tube tracker (TRT) covering $|\eta| < 2.0$, all sitting in an axial 2 T magnetic field provided by a superconducting solenoid. The sampling calorimetry is hermetic out to $|\eta| = 4.9$ and is generally divided into barrel ($|\eta| < 1.4$), endcap ($1.4 < |\eta| < 3.2$) and forward ($3.2 < |\eta| < 4.9$) regions. The highly-segmented electromagnetic (EM) calorimetry uses liquid argon with lead or copper absorber material and includes three longitudinal sampling layers in addition to a presampler for $|\eta| > 1.8$. The hadronic calorimetry uses scintillator tiles with steel absorber in the barrel ($|\eta| < 1.7$) and liquid argon (LAr) with copper (tungsten) absorber in the endcap (forward) region. A

[2] ATLAS uses a right-handed coordinate system with its origin at the nominal interaction point (IP) in the centre of the detector and the z-axis along the beam pipe. The x-axis points from the IP to the centre of the LHC ring, and the y-axis points upward. Cylindrical coordinates (r, ϕ) are used in the transverse plane, ϕ being the azimuthal angle around the beam pipe. The pseudorapidity is defined in terms of the polar angle θ as $\eta = -\ln\tan(\theta/2)$.

multi-level trigger system of dedicated hardware and software filters is used to select pp collisions of interest.

2.2 Object reconstruction

The reconstruction and definition of physics objects used in this analysis is detailed in Ref. [3], while an overview is presented in this section.

Vertices and tracks The event hard-scatter primary vertex is defined as the reconstructed vertex with the largest $\sum p_T^2$ of constituent tracks. In this analysis, only events where the reconstructed primary vertex is within $|\Delta z| < 0.1$ mm from the truth hard-scatter vertex are considered. For the physics processes considered, the reconstructed primary vertex matches the truth hard-scatter vertex more than 95% of the times. Tracks are required to have $p_{\mathrm{T}} > 0.5\,\mathrm{GeV}$ and to satisfy quality criteria designed to reject poorly measured and fake tracks. Tracks are assigned to vertices based on the track-to-vertex association resulting from the vertex reconstruction [4]. Other tracks are assigned to the nearest vertex based on the distance $|\Delta z \cdot \sin\theta|$, up to a maximum distance of 3.0 mm. Tracks not matched to any vertex are not considered. Tracks originating from the hard-scatter primary vertex and from pileup vertices are then assigned to jets using a technique known as ghost association [5].

Jets Calorimeter jets are reconstructed from topological clusters [6] using the local cluster weighting (LCW) algorithm [7]. FastJet 2.4.3 is used to reconstruct anti-k_t [8] jets with a distance parameter $R = 0.4$. Similarly, truth jets are reconstructed as anti-k_t $R = 0.4$ jets from stable[3] truth particles in the final state of the simulated hard-scatter (*truth hard-scatter jets*) or in-time pileup (*truth pileup jets*) interaction. Calorimeter jets are calibrated using pileup subtraction followed by a jet-energy-scale (JES) response correction, as described in detail in Refs. [3, 9]. Unless noted otherwise, jets are required to have $20\,\mathrm{GeV} < p_{\mathrm{T}} < 50\,\mathrm{GeV}$. *Central* jets are required to be within $|\eta| < 2.4$ and their charged particles are within the coverage of the inner tracking detector. *Forward* jets are in the region $2.4 < |\eta| < 4.9$ and the tracks associated to their charged particles are not measured.

As discussed in Sec. 3, the studies in this note require a classification of the reconstructed jets in three categories: hard-scatter jets, pileup QCD jets, and pileup stochastic jets. Jets are thus truth-labeled based on a matching criterion to truth jets. Similarly to Ref. [3] jets are first classified as hard-scatter or pileup jets. Jets are labeled as hard-scatter jets if a truth hard-scatter jet with $p_{\mathrm{T}} > 10\,\mathrm{GeV}$ [4] is found within $\Delta R = \sqrt{(\Delta\eta)^2 + (\Delta\phi)^2} < 0.3$. Jets are labeled as pileup jets if no truth hard-scatter jet with $p_{\mathrm{T}} > 4\,\mathrm{GeV}$ is found within $\Delta R > 0.6$. Pileup jets are further classified as QCD pileup if they are matched within $\Delta R < 0.3$ to a truth pileup jet with $p_{\mathrm{T}} > 10\,\mathrm{GeV}$. Otherwise, pileup jets are labeled as stochastic pileup jets if there are no truth pileup jets with $p_{\mathrm{T}} > 10\,\mathrm{GeV}$ within $\Delta R < 0.6$.

[3] Truth particles are considered stable if their decay length $c\tau$ is greater than 1 cm. A truth particle is considered to be interacting if it is expected to deposit most of its energy in the ATLAS calorimeters; muons and neutrinos are considered to be non-interacting.

[4] The $p_{\mathrm{T}} > 10\,\mathrm{GeV}$ threshold is used to avoid accidental matches of reconstructed jets with soft activity from the truth hard-scatter.

JVT The JVT discriminant is built out of the combination of two jet variables, corrJVF and R_{pT}, that provide information to separate hard-scatter from pileup jets. The quantity corrJVF is defined as

$$\mathrm{corrJVF} = \frac{\sum_k p_{\mathrm{T}}^{\mathrm{trk}_k}(\mathrm{PV}_0)}{\sum_l p_{\mathrm{T}}^{\mathrm{trk}_l}(\mathrm{PV}_0) + \frac{\sum_{m\geq 1}\sum_l p_{\mathrm{T}}^{\mathrm{trk}_l}(\mathrm{PV}_m)}{(k \cdot n_{\mathrm{trk}}^{\mathrm{PU}})}}. \tag{1}$$

where PV_i denotes the reconstructed event vertices (PV_0 is by convention the hard-scatter vertex), and $\sum_k p_{\mathrm{T}}^{\mathrm{trk}_k}(\mathrm{PV}_0)$ is the scalar p_{T} sum of the tracks that are associated with the jet and originate from the hard-scatter vertex. The term $p_{\mathrm{T}}^{\mathrm{PU}} = \sum_{i\geq 1}\sum_l p_{\mathrm{T}}^{\mathrm{trk}_l}(\mathrm{PV}_i)$ denotes the scalar p_{T} sum of the tracks associated with the jet and originating from pileup vertices. To correct for the linear increase of $\langle p_{\mathrm{T}}^{\mathrm{PU}}\rangle$ with the total number of pileup tracks per event ($n_{\mathrm{trk}}^{\mathrm{PU}}$), we divide $p_{\mathrm{T}}^{\mathrm{PU}}$ in the corrJVF definition by $(k \cdot n_{\mathrm{trk}}^{\mathrm{PU}})$ with $k = 0.01$. The variable R_{pT} is defined as the scalar p_{T} sum of the tracks that are associated with the jet and originate from the hard-scatter vertex divided by the fully calibrated jet p_{T}, which includes pileup subtraction:

$$R_{\mathrm{pT}} = \frac{\sum_k p_{\mathrm{T}}^{\mathrm{trk}_k}(\mathrm{PV}_0)}{p_{\mathrm{T}}^{\mathrm{jet}}}. \tag{2}$$

The JVT discriminant is built by defining a 2-dimensional likelihood based on a k-nearest neighbor (kNN) algorithm [10].

An extension of the R_{pT} variable computed with respect to any vertex i in the event, $R_{\mathrm{pT}}^i = \frac{\sum_k p_{\mathrm{T}}^{\mathrm{trk}_k}(\mathrm{PV}_i)}{p_{\mathrm{T}}^{\mathrm{jet}}}$, is also used in this analysis.

2.3 Samples

The studies presented in this note are performed using simulated pp collisions, at a center-of-mass energy $\sqrt{s} = 8$ TeV, yielding specific physics processes. QCD dijet events are produced with the Pythia8 generator (version 8.160) using the CT10 PDF set and the AU2 CT10 underlying-event tune [11]. Simulated $t\bar{t}$ events are generated with powheg box V1.0 [12–14] using the PDF set CT10 [15]. PYTHIA 6.4 [16] was used for fragmentation and hadronization with the Perugia2011C [17] tune that employs the LO CTEQ6L1 PDF set [18]. The $Z(\rightarrow \mu\mu)$+jets sample is generated with powheg box V1.0 and showered with Pythia8 [19]. For all samples, the effect of in-time as well as out-of-time pileup is simulated using minimum-bias events generated with Pythia8 to reflect the pileup conditions during the 2012 data-taking period. All generated events were processed with a detailed simulation of the ATLAS detector response [20] based on geant4 [21] and subsequently reconstructed and analyzed in the same way as the data.

3 Sources of pileup jets

The reconstruction of spurious jets from pileup interactions has two components: *QCD jets*, where the particles in the jet stem from a single pileup interaction, and *stochastic jets*, that combine particles from different vertices in the high density particle flow. Figure 1 shows an event with a hard-scatter jet, a QCD pileup jet and a stochastic pileup jet. The particles associated to the hard-scatter jet originate from the primary interaction. The particles associated with the QCD pileup jet originate all from the same pileup interaction. The stochastic pileup jet includes particles originating from different vertices, without a prevalent source.

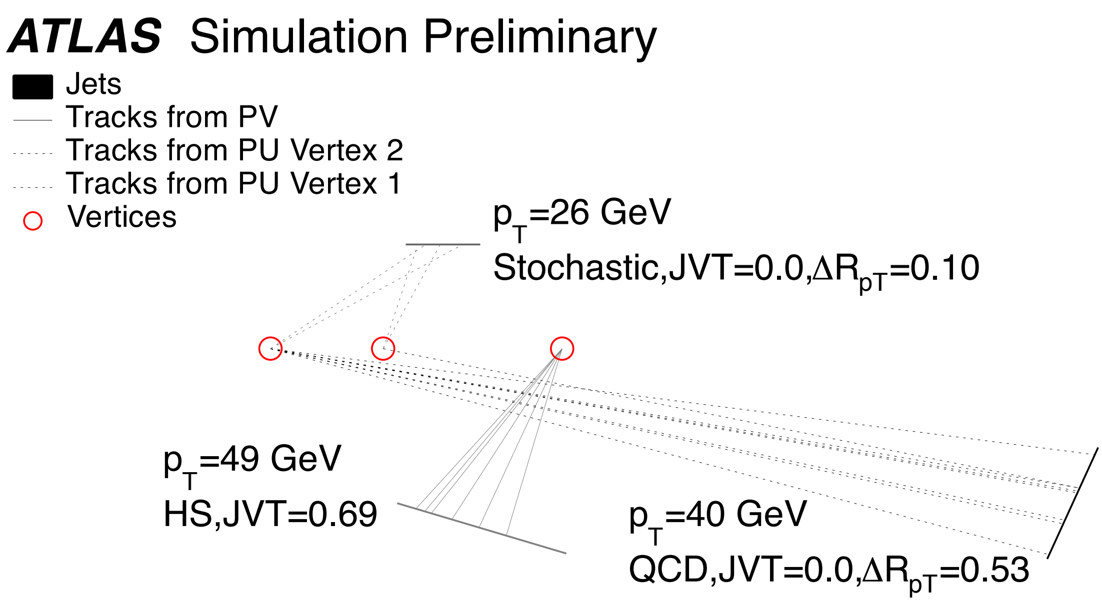

Figure 1: Example of an event containing a central hard-scatter (HS) jet, a central QCD pileup jet, and a central stochastic pileup jet. The p_{T}, JVT and ΔR_{pT} (see Sec. 3.1) values are quoted for each jet.

Figure 2 shows the fraction of QCD pileup jets as a function of the pseudorapidity and p_{T} of the jet and the number of pileup interactions. The fraction is defined as the ratio between the number of QCD pileup jets in a given pseudorapidity and p_{T} range and the total number of pileup jets in the same range. The fraction of QCD jets increases significantly in the forward region and it constitutes more than 80% of pileup jets with $p_{\mathrm{T}} > 30$ GeV overall. The fraction of stochastic jets becomes more prominent at low p_{T} as the number of interaction increases. The majority of pileup jets in the forward region are QCD pileup jets. Therefore, targeting QCD pileup jets is an important component of forward pileup mitigation.

3.1 A discriminant for pileup jet classification

As it will be discussed in Section 4, the rejection of forward QCD pileup jets relies on the discrimination between stochastic and QCD pileup jets in the central region using track and vertex information. This section describes a new discriminant built for this purpose.

The JVT successfully rejects both types of pileup jets, however the underlying features are different. Tracks associated to QCD jets are mostly originating from the same vertex corresponding to a pileup interaction, thus yielding small R^{0}_{pT} values with respect to the primary vertex. However such jets have large values of R^{i}_{pT} with respect to the pileup vertex i from which they originated. On the other hand, tracks associated to stochastic jets are equally likely to originate from any pileup interaction, thus yielding small R^{i}_{pT} values with respect to any vertex. This feature can be exploited to discriminate between the

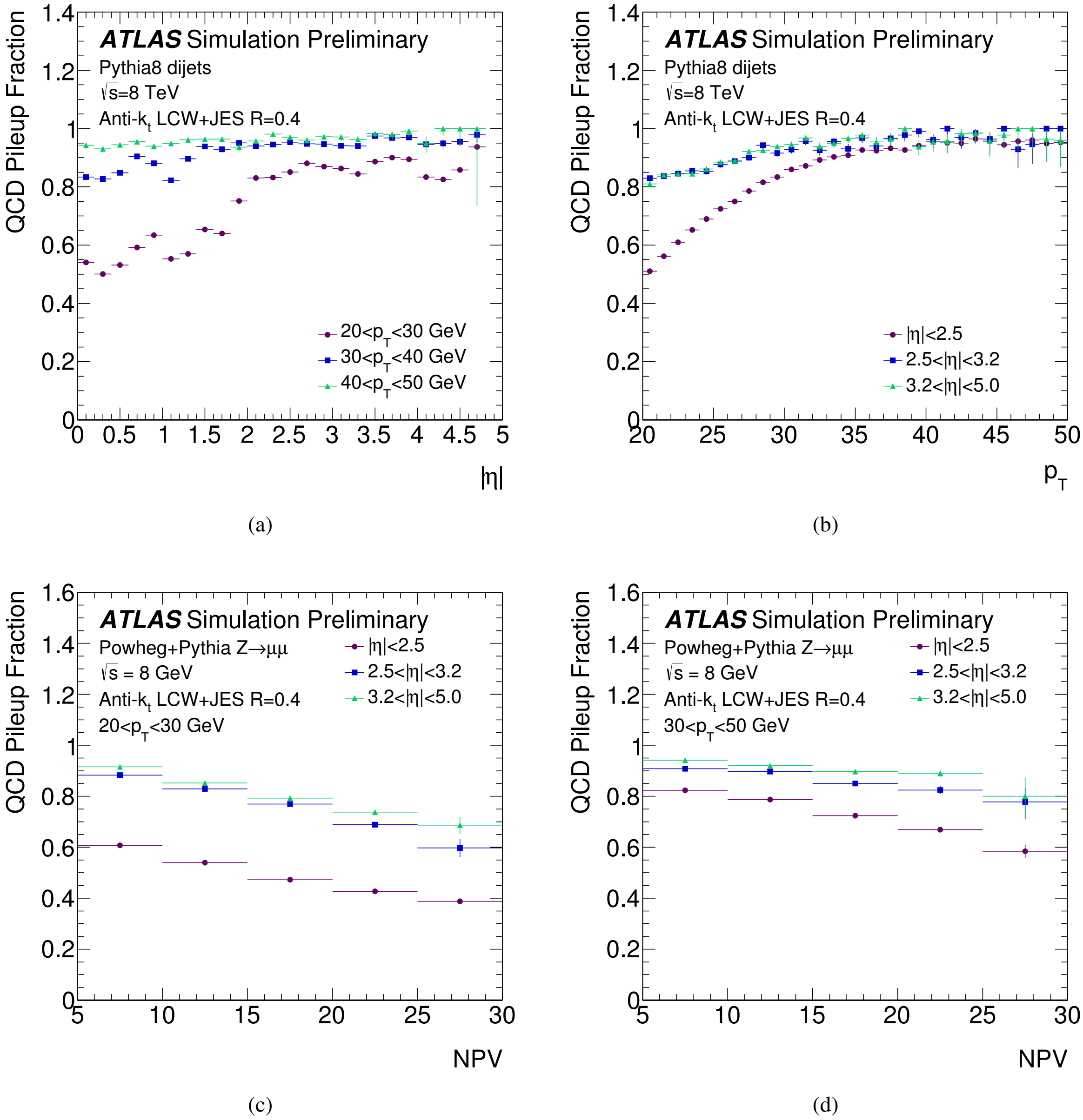

Figure 2: Fraction of pileup jets that are matched to a truth in-time pileup jet, as a function of η (a), p_{T} (b), and the number of reconstructed vertices in the event for jets with $20\,\mathrm{GeV} < p_{\mathrm{T}} < 30\,\mathrm{GeV}$ (c) and $30\,\mathrm{GeV} < p_{\mathrm{T}} < 50\,\mathrm{GeV}$ (d), as observed in dijet events with Pythia8 pileup simulation.

two categories. The two largest R^i_{pT} values are going to be of similar size for stochastic jets, while a large difference will show for QCD jets, as most tracks originate from the same pileup vertex.

Thus, the difference between the two leading R^i_{pT} [5] for a central jet, ΔR_{pT}, can be used for discriminating QCD pileup jets from stochastic pileup jets. The ΔR_{pT} distributions for stochastic and QCD jets, shown in Fig. 3, have different shapes with the distribution for stochastic jets peaking at zero. Therefore a minimum ΔR_{pT} requirement can effectively reject stochastic pileup jets. Since the fraction of stochastic pileup jets is significantly large only for central jets with $p_{\mathrm{T}} < 30$ GeV, as shown in Fig. 2, in the following the ΔR_{pT} requirement is applied only for those jets, while pileup central jets with $p_{\mathrm{T}} > 30$ GeV are assumed to be QCD pileup jets independently from their ΔR_{pT} value.

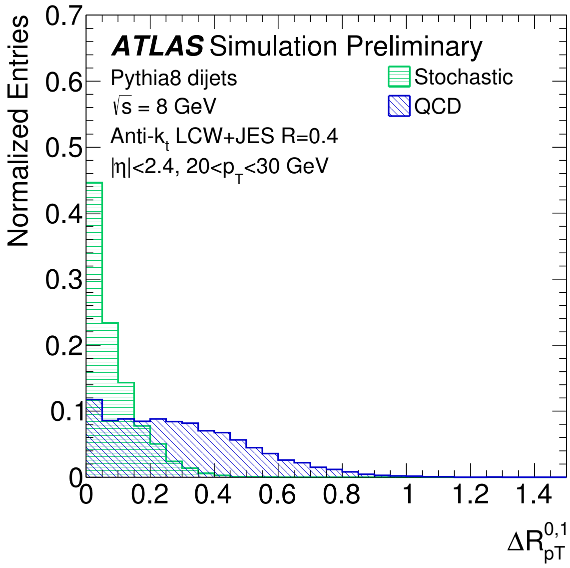

Figure 3: Distribution of ΔR_{pT} for stochastic and QCD pileup jets, as observed in dijet events with Pythia8 pileup simulation.

4 Forward JVT

While it has been shown that pileup mitigation techniques based on jet shape are effective in suppressing stochastic pileup jets [22], QCD pileup jets are prevalent in the forward region. Therefore developing an effective rejection method targeting specifically QCD pileup jets is of particular importance.

QCD pileup jets are mostly produced in pairs. Due to transverse momentum conservation, the two jets in the pair will have opposite directions in the transverse plane. This dijet correlation in the transverse plane can be exploited to identify QCD pileup jets beyond the coverage of the Inner Detector. Figure 4 shows an event with such a pair of QCD pileup jets, one within the Inner Detector coverage and the other in the forward region.

[5] The R^i_{pT} variable is found to be a better discriminant than the analogous corrJVF^i. In stochastic jets each pileup interaction contributes with few particles and R^i_{pT} is sensitive to the contribution of neutral particles.

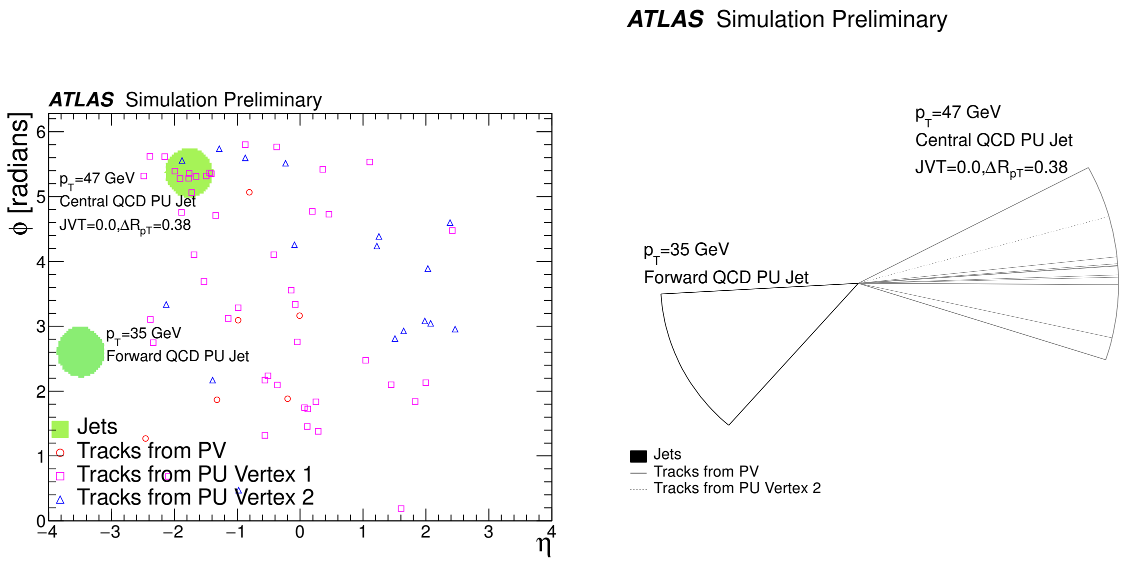

(a) (b)

Figure 4: η-ϕ (a) and rz (b) view of an event containing a forward QCD pileup jet and a central QCD pileup jet forming a back-to-back pair.

4.1 Algorithm

The procedure shown in Fig. 5, referred to as *forward* JVT (fJVT) is used to suppress forward pileup jets. The main parameters for the forward JVT algorithm are thus the threshold JVT_{max} to select central pileup jets and the minimum ΔR_{pT} requirement to select QCD pileup jets. JVT_{max} is set to 0.05 corresponding to an efficiency of selecting pileup jets of 95%. The minimum ΔR_{pT} requirement defines the operating point in terms of hard-scatter and pileup efficiencies. The $|\Delta\phi| > \pi - 1$ requirement ensures that the central jet is in the opposite hemisphere in the central plane. The requirement is sufficiently loose that most of the QCD dijet pairs pass the selection.

4.2 Performance

Figure 6 shows the efficiency of selecting pileup forward jets (*Forward PU Fake Rate*) as a function of the efficiency of selecting hard-scatter forward jets (*Forward HS Efficiency*) when varying the minimum ΔR_{pT} requirement for central jets with $p_{\mathrm{T}} < 30\,\mathrm{GeV}$. The acceptance for central jets also plays an important role. Reconstructing central jets with minimum p_{T} (referred to as $p_{\mathrm{T}}{}^{\mathrm{central}}$) of 10 GeV[6] allows achieving significantly lower rates of forward QCD pileup jets at only slightly lower hard-scatter efficiencies. The lower $p_{\mathrm{T}}{}^{\mathrm{central}}$ threshold increases the probability of reconstructing the central jet in the pileup QCD dijet process, thus improving the efficiency of identifying and rejecting forward pileup QCD jets. However, the larger number of reconstructed central jets increases the rate of accidental matching for hard-scatter forward jets, thus reducing the hard-scatter efficiency. In the following the lower $p_{\mathrm{T}}{}^{\mathrm{central}} > 10$ GeV re-

[6] As discussed in Sec. 2.2, the miminum p_{T} for jets is typically 20 GeV.

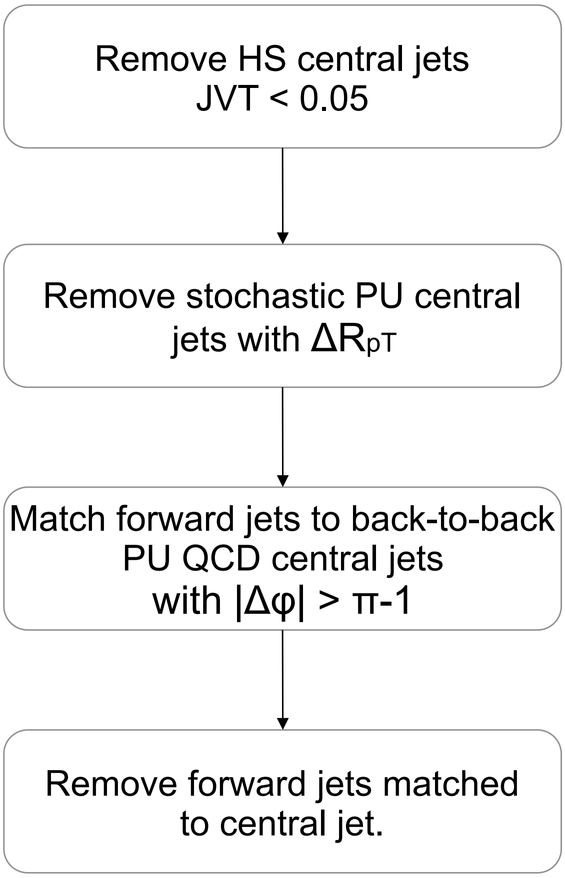

Figure 5: The forward JVT algorithm. Pileup and hard-scatter jets are referred to as PU and HS, respectively.

quirement is used for the fJVT requirement with hard-scatter efficiency of 85%, while the 94% efficiency is achieved with ${p_{\mathrm{T}}}^{\mathrm{central}} > 20$ GeV.

Using a minimum ΔR_{pT} of 0.18, hard-scatter efficiencies of 94% and 85% are achieved for pileup fake rates of respectively 75% and 60%, considering jets with $20\,\mathrm{GeV} < p_{\mathrm{T}} < 50\,\mathrm{GeV}$. The dependence of the hard-scatter and pileup efficiencies on the forward jet p_{T} is shown in Fig. 7. Since the JVT_{max} requirement removes central hard-scatter jets, the hard-scatter forward jets inefficiency is only due to accidental matching with central pileup jets, which does not depend on the p_{T} of the forward hard-scatter jet. On the other hand, the hard-scatter efficiency depends on the number of pileup interactions, as shown in Fig. 8, as harsher pileup conditions increase the chance of accidental matching. The pileup rate depends on the p_{T} of the forward jets, due to the p_{T}-dependence of the QCD fraction, shown in Fig. 2.

Figure 9 shows the dependence of the average jet multiplicity as a function of the number of reconstructed primary vertices in $Z(\rightarrow \mu\mu)$+jets events. Events are required to contain a Z boson candidate with p_{T} >30 GeV and at least one truth hard-scatter forward jet. The jet multiplicity is computed by counting the reconstructed forward jets with p_{T} >20 GeV and p_{T} >30 GeV. The fJVT requirements reduces the slope of the dependence, which is removed entirely for jets with $p_{\mathrm{T}} > 30$ GeV with the 85% efficient fJVT requirement.

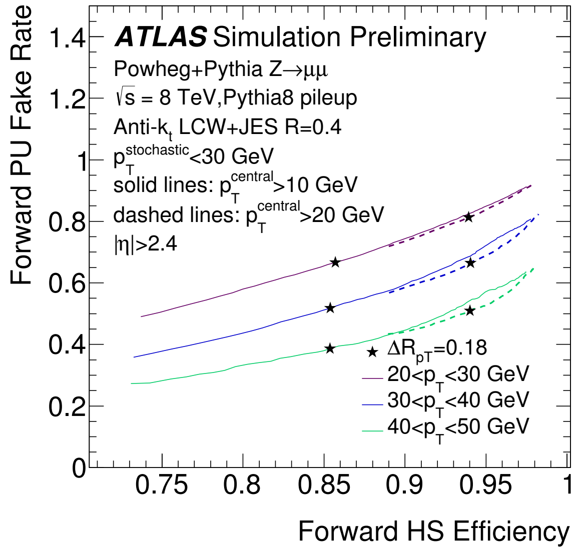

Figure 6: ROC curves corresponding to a scan of the ΔR_{pT} requirement for a minimum central jet p_{T} of 20 and 10 GeV, respectively. The starred points correspond to the two chosen operating points.

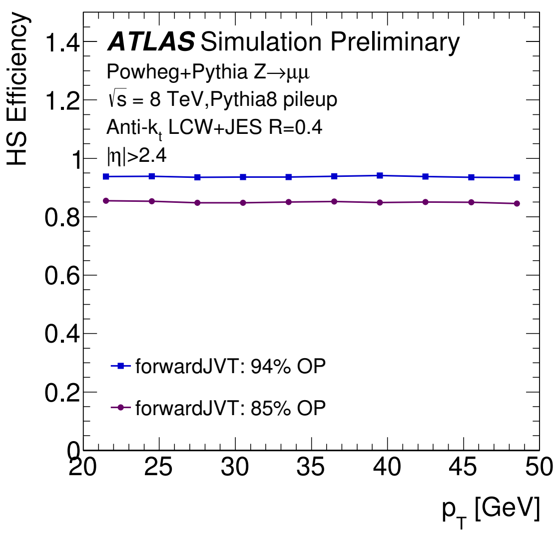

(a)

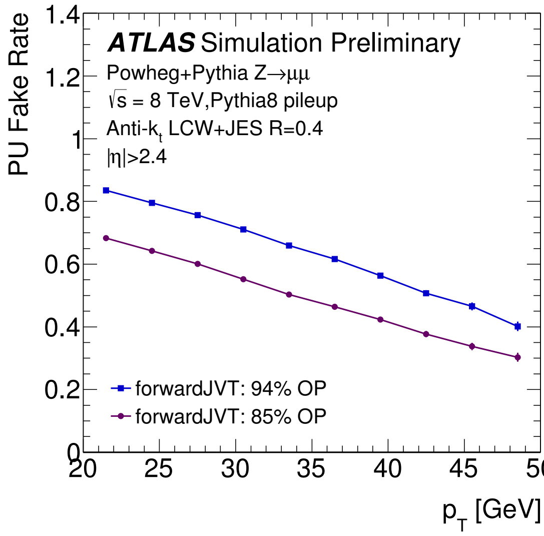

(b)

Figure 7: Hard-scatter efficiency (a) and pileup rate (b) as a function of the forward jet p_{T}.

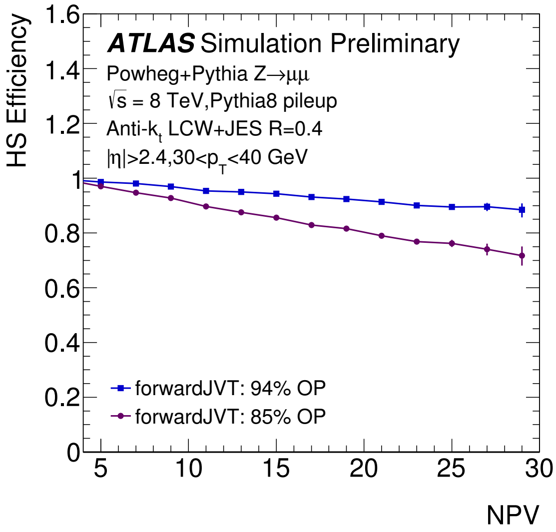

(a)

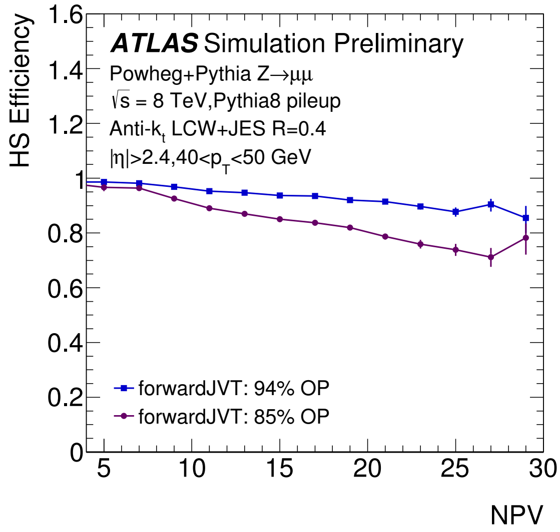

(b)

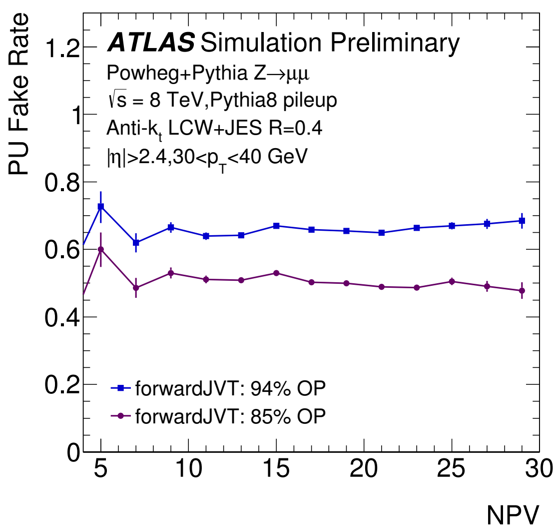

(c)

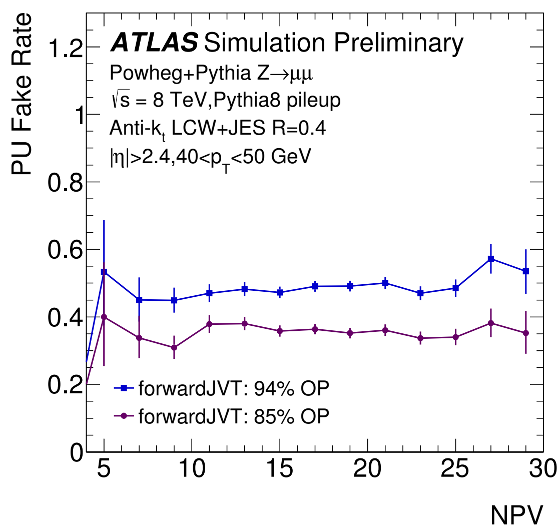

(d)

Figure 8: Hard-scatter efficiency (a)(b) and pileup rate (c)(d) as a function of the number of reconstructed vertices in the event, for forward jets with 30 GeV $< p_{\mathrm{T}} <$ 40 GeV (a)(c) and 40 GeV $< p_{\mathrm{T}} <$ 50 GeV (b)(d).

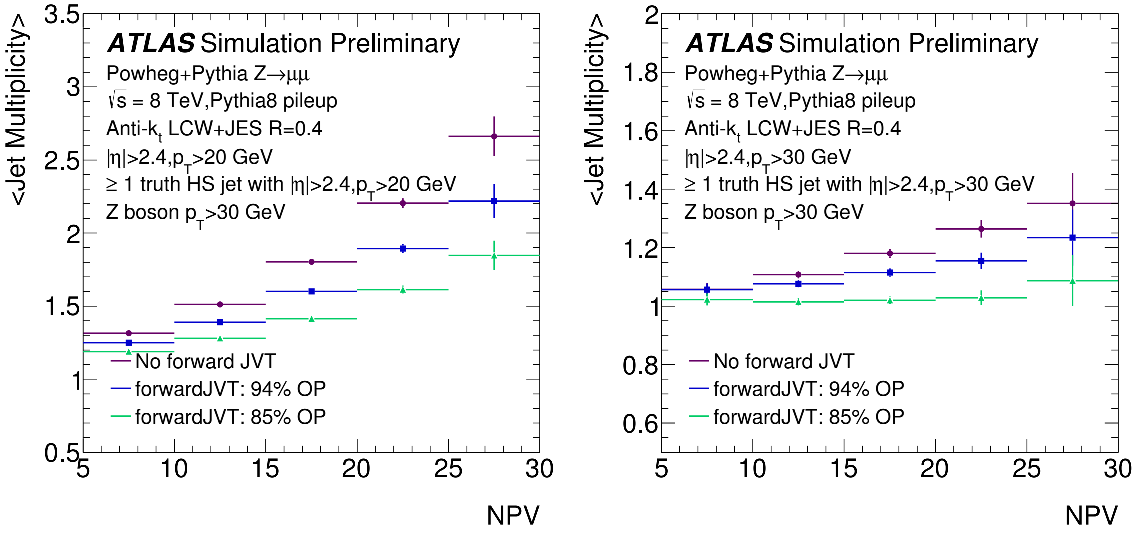

(a) (b)

Figure 9: Average multiplicity of forward jets with $p_T > 20$ GeV (a) and $p_T > 30$ GeV (b) as a function of the number of reconstructed vertices.

5 Process dependence

The potential dependence of forward JVT on the physics process is studied by comparing the performance of the method in $Z(\rightarrow \mu\mu)$+jets events and in $t\bar{t}$ events. The pileup efficiencies as a function of the hard-scatter efficiencies are shown in Fig. 10. When using a lower p_T threshold of 10 GeV for selecting central pileup jets the difference in performance between $Z(\rightarrow \mu\mu)$+jets and $t\bar{t}$ events is small, suggesting that the forward JVT technique is not sensitive to the hard-scatter jet topology or kinematics. Additional studies comparing different generators and simulation tunings, and simulated and data samples, will have to be performed in order to calibrate the algorithm performance and assess the associated uncertainties.

6 Conclusions

Forward JVT is a new technique developed for the suppression of pileup jets in the forward region. The method exploits the correlation of QCD pileup jets in the transverse plane and extrapolates JVT, track and vertex based, beyond the coverage of the Inner Detector. Forward JVT relies on a new variable, ΔR_{pT}, that allows discrimination between stochastic and QCD pileup jets. In samples with Pythia8 pileup simulation, he technique reduces the overall forward pileup jet rate by 25% and 40% for hard-scatter efficiencies of 94% and 85%, respectively. The hard-scatter efficiency does not depend on the jet p_T, while a dependence on the number of reconstructed primary vertices is observed. The efficiency decreases by 1% and 0.3% per reconstructed vertex, for overall efficiencies of 94% and 85%, respectively. The pileup rate significantly decreases with increasing jet p_T, while it does not depend on the number of reconstructed primary vertices. No significant dependence on the physics process has been observed.

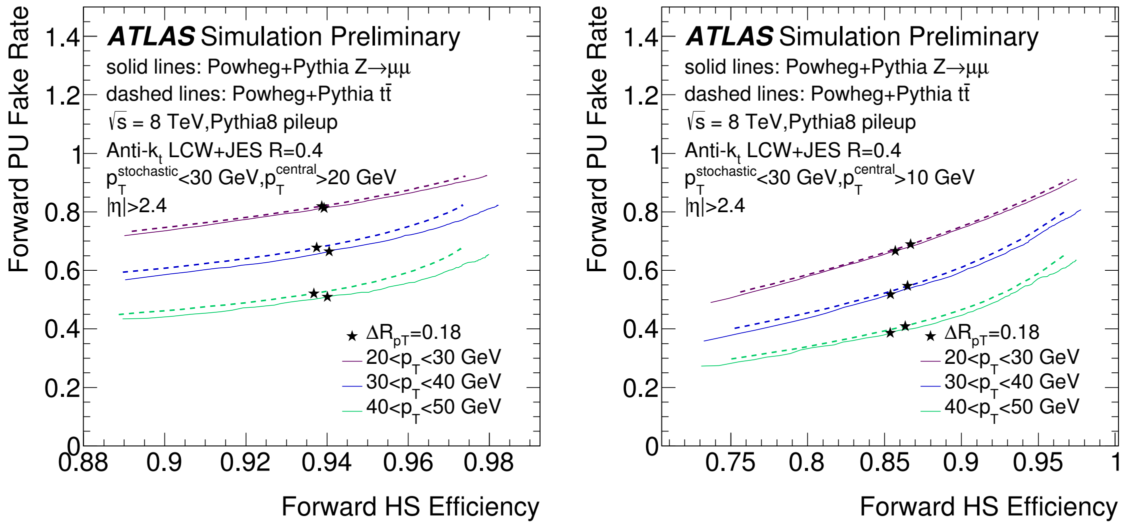

(a) (b)

Figure 10: ROC curves for $Z(\rightarrow \mu\mu)$+jets and $t\bar{t}$, superimposed, for fJVT with $p_{\mathrm{T}}{}^{\mathrm{central}} > 20\,\mathrm{GeV}$ (a) and $p_{\mathrm{T}}{}^{\mathrm{central}} > 10\,\mathrm{GeV}$ (b).

Forward JVT provides a new capability for pileup suppression in ATLAS, enabling, for the first time, the identification and removal of fake pileup jets outside the tracker acceptance.

References

[1] ATLAS Collaboration, *The ATLAS Experiment at the CERN Large Hadron Collider*, JINST **3** (2008) S08003.

[2] ATLAS Collaboration, *Tagging and suppression of pileup jets with the ATLAS detector*, ATLAS-CONF-2014-018, 2014, URL: https://cds.cern.ch/record/1700870.

[3] ATLAS Collaboration, *Pile-up subtraction and suppression for jets in ATLAS*, ATLAS-CONF-2013-083, 2013, URL: https://cds.cern.ch/record/1570994.

[4] ATLAS Collaboration, *Performance of the ATLAS Inner Detector Track and Vertex Reconstruction in the High Pile-Up LHC Environment*, ATLAS-CONF-2012-042, 2012, URL: https://cdsweb.cern.ch/record/1435196.

[5] M. Cacciari, G. P. Salam and G. Soyez, *The Catchment Area of Jets*, JHEP **0804** (2008) 005, arXiv: 0802.1188 [hep-ph].

[6] W Lampl et al., *Calorimeter Clustering Algorithms: Description and Performance*, ATL-LARG-PUB-2008-002, 2008, URL: https://cds.cern.ch/record/1099735.

[7] T Barillari et al., *Local Hadronic Calibration*, ATL-LARG-PUB-2009-001-2, 2008, URL: https://cds.cern.ch/record/1112035.

[8] M. Cacciari, G. P. Salam and G. Soyez, *The anti-k_t jet clustering algorithm*, JHEP **0804** (2008) 063, arXiv: 0802.1189 [hep-ph].

[9] ATLAS Collaboration, *Jet energy measurement with the ATLAS detector in proton-proton collisions at $\sqrt{s} = 7$ TeV*, Eur. Phys. J. **C73** (2013) 2304, arXiv: 1112.6426 [hep-ex].

[10] A. Hoecker et al., *TMVA: Toolkit for Multivariate Data Analysis*, PoS **ACAT** (2007) 040, arXiv: physics/0703039.

[11] *Summary of ATLAS Pythia 8 tunes*, ATL-PHYS-PUB-2012-003, 2012, URL: https://cds.cern.ch/record/1474107.

[12] S. Alioli et al., *A general framework for implementing NLO calculations in shower Monte Carlo programs: the POWHEG BOX*, JHEP **1006** (2010) 043, arXiv: 1002.2581 [hep-ph].

[13] S. Frixione, P. Nason and C. Oleari, *Matching NLO QCD computations with Parton Shower simulations: the POWHEG method*, JHEP **0711** (2007) 070, arXiv: 0709.2092 [hep-ph].

[14] P. Nason, *A New method for combining NLO QCD with shower Monte Carlo algorithms*, JHEP **0411** (2004) 040, arXiv: hep-ph/0409146 [hep-ph].

[15] H.-L. Lai et al., *New parton distributions for collider physics*, Phys. Rev. **D82** (2010) 074024, arXiv: 1007.2241 [hep-ph].

[16] T. Sjostrand, S. Mrenna and P. Z. Skands, *PYTHIA 6.4 Physics and Manual*, JHEP **0605** (2006) 026, arXiv: hep-ph/0603175 [hep-ph].

[17] P. Z. Skands, *Tuning Monte Carlo Generators: The Perugia Tunes*, Phys. Rev. **D82** (2010) 074018, arXiv: 1005.3457 [hep-ph].

[18] J. Pumplin et al., *New generation of parton distributions with uncertainties from global QCD analysis*, JHEP **0207** (2002) 012, arXiv: hep-ph/0201195 [hep-ph].

[19] T. Sjostrand, S. Mrenna and P. Z. Skands, *A Brief Introduction to PYTHIA 8.1*, Comput. Phys. Commun. **178** (2008) 852–867, arXiv: 0710.3820 [hep-ph].

[20] ATLAS Collaboration, *The ATLAS Simulation Infrastructure*, Eur. Phys. J. **C70** (2010) 823–874, arXiv: 1005.4568 [physics.ins-det].

[21] S. Agostinelli et al., *GEANT4: A Simulation toolkit*, Nucl. Instrum. Meth. **A506** (2003) 250–303.

[22] CMS Collaboration, *Pileup Jet Identification*, CMS-PAS-JME-13-005, 2013, URL: https://cds.cern.ch/record/1581583.